An Automated Variable E-Field DFT Application (A.V.E.D.A.) for Evaluation of Optimally Oriented Electric Fields on Chemical Reactivity

*Dalton J. Hanaway, C. Rose Kennedy**

Department of Chemistry, University of Rochester, Rochester, New York 14627, United States

ABSTRACT: Recent theoretical work and experiments at molecular junctions have provided a strong conceptualization for the effects of oriented electric fields (OEFs) on organic reactions. Depending upon the axis of application, OEFs can increase (or decrease) reaction rate or distinguish between isomeric pathways. Despite the conceptual elegance of OEFs, which may be applied externally or induced locally, as tools for catalyzing organic reactions, implementation in synthetically relevant systems has been hampered by inefficiencies in evaluating reaction sensitivity to field effects. Herein we describe the development of the Automated Variable Electric-Field DFT Application (A.V.E.D.A.) for streamlined evaluation of a reaction's susceptibility to OEFs. This open-source software was designed to be accessible for non-expert users of computational and programming tools. Following initiation by a single command (and with no subsequent intervention) the Linux workflow manages a series of density functional theory (DFT) calculations and mathematical manipulations to optimize local-minimum and transition-state structures in oriented electric fields of increasing magnitude. The resulting molecular and

reaction dipole moments, field-perturbed geometries, and net effective activation energies are compiled for user interpretation. Ten representative pericyclic reactions that showcase the development and evaluation of A.V.E.D.A. are described.

1. INTRODUCTION

Achieving precise control over reactivity and selectivity is a defining goal of synthetic chemistry. Traditionally, this has been achieved through substrate, reagent, or catalyst control under carefully tuned reaction conditions including (for example) solvent, concentration, temperature, and time. By contrast, external electromagnetic stimuli have traditionally been relegated to spectroscopic characterization with little consideration for potential effects on chemical transformations more broadly. In a disruption to these traditional approaches, oriented electric fields (OEFs) have been identified as an alternative synthetic tool.[1-4] An applied electric field hyper-polarizes co-axial bonds, which in turn alters the effective barriers for transformations involving changes in bonding and redistribution of electron density associated.[4] This phenomenon—called the electric field effect—has long been invoked to justify the catalytic efficiency of enzymes,[5-11] and spectroscopic work has quantified the field-induced component of enzymatic catalysis.[6, 12-16] Analogous techniques have been applied to probe effective electric field magnitude and orientation at electrode surfaces and interfaces.[17-19]

In non-enzymatic systems, theoretical studies, most commonly examining concerted cycloaddition reactions, support the viability of OEFs as unconventional "catalysts" for synthetically relevant transformations (Figure 1A).[20-23] In agreement with computational predictions, single-molecule experiments examining Diels–Alder substrates immobilized at molecular junctions supported that C–C bond formation was accelerated or inhibited depending

upon the orientation of the applied electric field (Figure 1A/B).[24, 25] Increasingly, this approach has been expanded to evaluate field effects on a range of chemical transformations at molecular junctions.[26-28] These studies further highlight sensitivity of OEF effects to alignment with the reaction axis, which is defined by the vector difference in electron localization between ground and transition states.[2, 25]

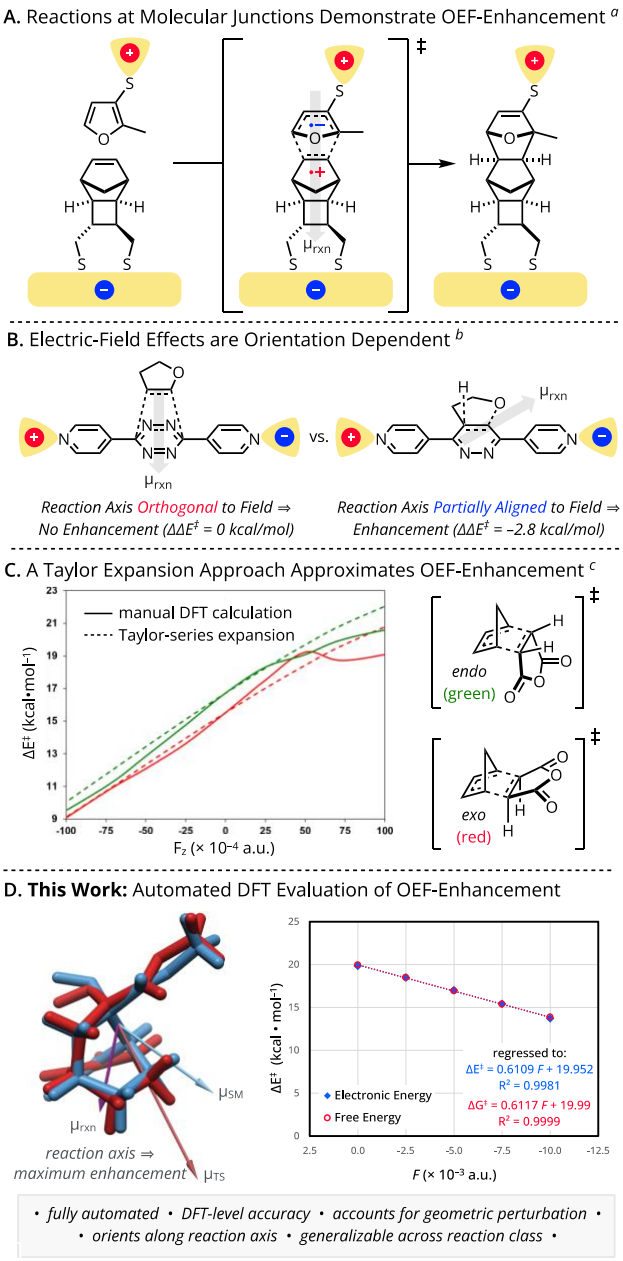

Figure 1. Foundational (A) conceptualization, (B) demonstration, and (C/D) approaches for expedited modeling of oriented electric field (OEF) effects on organic reactions. [a] Ref. 25 [b] Ref. 24 [c] Ref. 29. Plot modified with permission. ©2021 The Authors. Published by the American Chemical Society. For overlaid structures, blue = starting material local-minimum stationary point, red = lowest energy transition-state structure.

Electric field effects on molecular systems can be described mathematically through a power series where electronic energy (E) depends on interaction of the electric field ($\vec{F}$) with the molecular dipole moment ($\vec{\mu}$), polarizability ($\vec{\alpha}$), hyperpolarizability ($\vec{\beta}$), etc.[29, 30]

$$E(\vec{F}) = E_0 - \vec{\mu}\vec{F} - \frac{\vec{\alpha}}{2}\vec{F}^2 - \frac{\vec{\beta}}{6}\vec{F}^3 \cdots \quad (1)$$

As a first approximation, the higher-order terms can be neglected to relate the interaction energy to the product of the field and molecular dipole moment.

$$\Delta E \propto \vec{\mu}\vec{F} \quad (2)$$

Because both $\vec{\mu}$ and $\vec{F}$ are vectors, the effect is greatest when they are aligned parallel or anti-parallel. For a chemical reaction within an electric field, the vector difference in dipole moments between the local-minimum and transition-state structures ($\Delta\vec{\mu}^{\ddagger}$) therefore determines the overall change in energy barrier.

$$\Delta\Delta E^{\ddagger} \propto \Delta\vec{\mu}^{\ddagger}\vec{F} \quad (3)$$

For additional introduction into the fundamental bases for electric field effects on reactivity and their sensitivity to orientation, readers are referred to Shaik's tutorial review.[2, 3]

The theoretical understanding and proof-of-principle results described above have inspired a burgeoning area of research that seeks to harness OEFs in synthetically practical systems. This has been pursued through design of molecular capacitors,[31, 32] electrostatically biased molecular frameworks, and especially small-molecule reagents or catalysts with induced local electric field.[3, 33, 34] Related work in inorganic and coordination chemistry has employed secondary coordination sphere electrostatics to alter redox thermochemistry and related processes.[35-43] However,

harnessing (and understanding) even local field effects for synthetically useful reactivity is hampered by the tedious and technically arduous computational process of evaluating both the viability (magnitude of the possible electric field effect) and optimal orientation of the applied field.

Herein, a user-friendly application is presented to facilitate density functional theory (DFT) calculations of chemical reactions in the presence of optimally oriented electric fields. The Automated Variable Electric Field DFT Application (A.V.E.D.A.) provides the first fully automated electric field probe with DFT-level rigor. This approach is complementary to the Taylor-series expansion methodology developed by Luis and Torrent-Sucarrat,[44] which offers the trade-off between reduced precision and expedited computational efficiency when compared to DFT approaches (Figure 1C). Because each calculation with A.V.E.D.A. requires only a single command with simple user specifications that obviate the need for mathematical or programming expertise, this program is well-suited both as a teaching tool and as a pre-screening tool for experimental electric field applications. Building from the marked OEF effects observed for Diels–Alder reactions, the development and application of A.V.E.D.A. is showcased with a suite of non-cycloaddition pericyclic reactions as model transformations (Figure 1D).[45] Predictions obtained with A.V.E.D.A. support the broad viability of energetically significant electric-field effects across these families of pericyclic processes, despite their limited sensitivity to traditional forms of catalysis. Additional extensions to mechanistically distinct test cases demonstrate excellent transferability of the developed method.

2. RESULTS AND DISCUSSION

2.1. Input and Workflow

To develop the workflow for A.V.E.D.A. and evaluate OEF results, pericyclic reactions were identified as an attractive model reaction class.[45] Promising results obtained for the Diels–Alder reaction in an OEF suggested viability for a super-set of pericyclic reactions. Ten transformations—Cope elimination, Cope rearrangement, Claisen rearrangement, ene reaction, electrocyclic ring-opening/closing, and sigmatropic rearrangements ([1,5], [3,3], and [2,3])—were selected as the development data set in addition to the well-studied [4+2]-cycloaddition of cyclopentadiene and maleic anhydride.[20, 22, 44] The small size and concerted mechanisms enabled quick computation times and efficient algorithm development while offering a range of electronic descriptions and activation energies. Two representative transformations are depicted in the main text to illustrate the capabilities and results obtained with A.V.E.D.A. (Scheme 1). The remainder are provided in the Supporting Information.

Scheme 1. Select model reactions used to develop and demonstrate A.V.E.D.A. capabilities. [a]

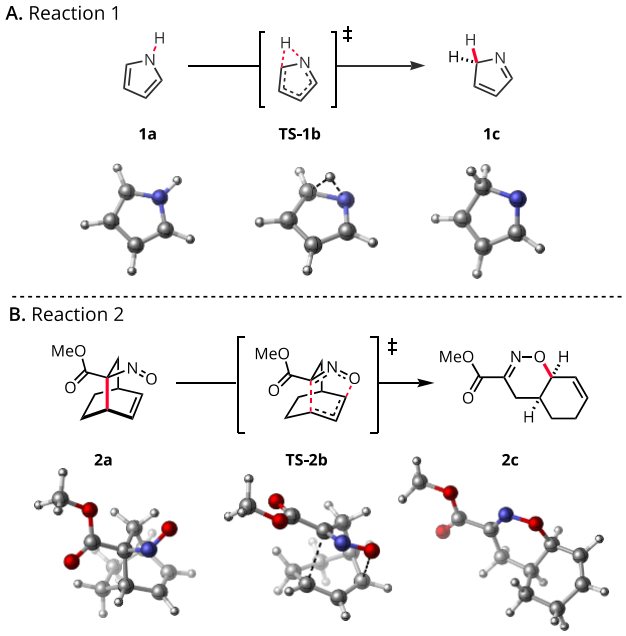

[a] H = white, C = gray, N = blue, O = red

A.V.E.D.A. input consists of two *.xyz* files listing the coordinates for local-minimum and transition-state structures for the transformation of interest. Output consists of optimized structures and energies at zero field and four non-zero electric field strengths. Note that the transition state describes a first-order saddle point on the ground-state potential energy surface, and the local minimum describes the nearest starting material or intermediate stationary point on the same energy surface. Upon instantiation, all subsequent OEF calculations proceed automatically with no user intervention required; see Computational Methods Section for details and Supporting Information for workflow visualization. Nonetheless, the quality of the output depends on the input, and users are encouraged to perform a routine optimization at a low level of theory and validate the stationary points by frequency analyses for input structures prior to submission through A.V.E.D.A. For reactions that could conceivably react through multiple conformers and/or include multiple elementary steps, each case should be evaluated independently. For example, the input structures for the model reactions described in this manuscript were optimized initially with B3LYP/6-31g(d) prior to submission to A.V.E.D.A. for evaluation at higher levels of theory.

Upon beginning each run, a directory containing copies of all necessary A.V.E.D.A. scripts is created. Local-minimum and transition-state structures are formatted into Gaussian input files for initial optimization in the absence of an applied electric field and submitted to SLURM for job handling.[46] The Gaussian computational chemistry package was selected due to its user-friendly interface, broad adoption by the synthetic community, and track-record of implementation in prior computational reports for investigating electric field effects.[1, 21, 23, 29, 47-50] Next, corresponding atoms in the optimized local-minimum and transition-state structures are aligned in the Cartesian coordinate system using PyMol, an open-source molecular visualization platform, via a root-mean-square deviation (RMSD) distance reduction.[51]

2.2 Reordering Atomic Coordinates

Subsequent calculations in an applied electric field utilizing the *Field* keyword must be performed on structures in Z-matrix format. In contrast to a Cartesian format, the Z-matrix constrains rotational degrees of freedom by constraining *atom 1* at the origin, *atom 2* on the z-axis, *atom 3* on the x-axis, and *atom 4* on the y-axis. These four atoms are referred to as the "orientation atoms" throughout this work. This constraint is necessary to prevent reorientation during the OEF optimization. During development, it became clear that the input order of atomic coordinates (and therefore the quality of the Z-matrix) influenced the success of subsequent OEF optimization steps. To support successful implementation, the atomic coordinates for aligned structures were thus reordered by one of three methods, described below.

- *Method 0* imposes no reordering criteria prior to implementation of the Gaussian *newzmat* utility. However, the *newzmat* utility may arbitrarily reorder the atomic coordinates if the input order is not conducive to z-matrix construction.

- *Method 1* was developed to maximize the stability of the orientation atoms in an electric field by calculating the unweighted Cartesian center of the transition structure and moving the nearest three atoms to the orientation atom positions prior to implementation of the *newzmat* utility. It is predicted these core atoms will have the smallest net displacement during optimization.

- *Method 2* reorders atoms to minimize impact of geometric changes on dipole orientation by designating the atom furthest from the site of transformation as orientation *atom 1* prior to implementation of the *newzmat*. This remote atom and all subsequent atoms are moved

in a block to the top of the input file so that connectivity represented by atom order is preserved with minimal perturbation.

During testing on the pericyclic data set, it was determined that *method 1* was most suitable when fringe atoms could easily rotate (e.g. a methyl group) or when the transition state was comprised of two unconnected fragments associated only by bond-breaking and forming (see Supporting Information for details). *Method 2* proved useful when *method 1* produced a low-quality Z-matrix due to inconsistencies between atom order and molecular connectivity.

2.3 Dipole Moment Vector Algebra

Following alignment and reordering, single-point energy calculations are performed in the Cartesian and Z-matrix input formats for both the optimized local-minimum and transition-state structures. From these results, A.V.E.D.A. calculates the optimal electric field alignment from the normalized dipole difference vector ($\vec{\mu}^{\ddagger}$or $\vec{\mu}_{rxn}$) between the local-minimum ($\vec{\mu}_{Int}$) and transition-state ($\vec{\mu}_{TS}$) dipole moments (eq. 4, Figure 2). This unit vector ($\hat{\mu}^{\ddagger}$), often described as the "reaction axis", points along the flow of electron density during a transformation and thus approximates the orientation most susceptible to beneficial electric field perturbation.[20]

$$\hat{\mu}^{\ddagger} = \frac{\vec{\mu}_{TS,cart} - \vec{\mu}_{Int,cart}}{\|\vec{\mu}_{TS,cart} - \vec{\mu}_{Int,cart}\|} \quad (4)$$

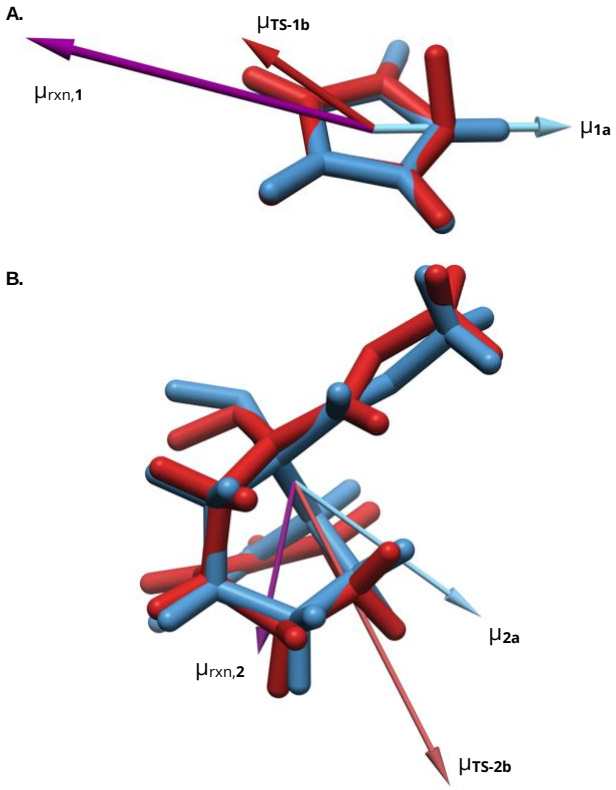

Figure 2. Structural alignment and vector algebra to determine the reaction dipole ($\vec{\mu}^{\ddagger}$or $\vec{\mu}_{rxn}$) and normalized reaction axis ($\hat{\mu}^{\ddagger}$) from the local-minimum (blue) and transition-state (red) structures for (A.) Reaction 1 and (B.) Reaction 2. The electric field is applied along the negative direction of $\hat{\mu}^{\ddagger}$.

However, the local-minimum and transition-state structures change orientation independently when converted from Cartesian to Z-matrix coordinate systems. Therefore, $\hat{\mu}^{\ddagger}$ must be mapped between the two orientations for each structure. This process is accomplished by generating rotation matrices for the local-minimum and transition-state dipole moments (eq. 5–7). For each structure, the Cartesian $\hat{\mu}^{\ddagger}_{cart}$ vector is translated with its corresponding rotation matrix (eq. 7) into the Z-matrix coordinate system. The electric field is then applied along the resulting $\hat{\mu}^{\ddagger}_{zmat,SM}$ or $\hat{\mu}^{\ddagger}_{zmat,TS}$ for the local-minimum and transition-state structures respectively.

$$\mathbf{v} = \hat{\mu}^{\ddagger}_{cart} \times \hat{\mu}^{\ddagger}_{zmat} \tag{5}$$

$$\mathbf{v}_{\times} = \begin{bmatrix} 0 & -v_3 & v_2 \\ v_3 & 0 & -v_1 \\ -v_2 & v_2 & 0 \end{bmatrix} \tag{6}$$

$$\mathbf{R}_{cart \to zmat} = \mathbf{I}_3 + \mathbf{v}_{\times} + (\mathbf{v}_{\times} \cdot \mathbf{v}_{\times}) \left(\frac{1 - \left(\hat{\mu}^{\ddagger}_{cart} \cdot \hat{\mu}^{\ddagger}_{zmat} \right)}{\|\mathbf{v}\|^2} \right) \tag{7}$$

2.4. Job Submission and Output

Gaussian submission scripts are generated for geometry optimizations with applied electric fields oriented along $\hat{\mu}^{\ddagger}_{zmat}$ and scaled by −2.5, −5.0, −7.5, and −10.0 × 10^{-3} a.u. The structures optimized at zero-field (above) are used to generate the input geometry for the −2.5 × 10^{-3} a.u case. Input geometries for subsequent optimizations at greater field strengths are called recursively from the preceding checkpoint files once optimization in the weaker field converges. This iterative approach improves the probability of successful computational outcomes by minimizing the geometric perturbation in any single step. After all eight OEF optimizations have converged, the output files are moved to the Results directory for analysis. At this stage, the RMSD structural deviation for each optimized structure is calculated with respect to the unperturbed (zero-field) system and reported in the output. Deviations of the RMSD >10% thus warn the users of possible changes to mechanism, fragmentation, and/or field-induced distortions.[21, 48, 49]

Using A.V.E.D.A., all eleven pericyclic reactions in the development data set were evaluated using four different functionals (B3LYP, B3LYP-D3, M06-2X, and ωB97X-D) and Weigend's triple-ζ basis set, def2TZVP.[52, 53] The hybrid B3LYP functionals[54] (with and without Grimme's D3 empirical dispersion correction)[55] and M06-2X[56] (which accounts for dispersion intrinsically)

were selected due to their computational efficiency and track-record of performance for pericyclic reactions.[57, 58] The ωB97X-D variation of pure functional B97 was also evaluated to consider alternative functional forms with long-range dispersion correction.[59, 60] For each case, A.V.E.D.A. produced outputs resembling those illustrated in Figure 3 for Reaction 2 (see Supporting Information). However, the success rate varied with respect to the atomic ordering method selected. A successful run was characterized by near-linear reductions in activation energy as a function of OEF magnitude—indicated by an R^2 greater than 0.95 and no discontinuous jumps in energy or molecular geometry—with appropriate imaginary vibrational frequencies for intermediates (none) and transition states (one). Slight, continuous deviations from linearity can be expected from the higher order terms in eq. 1. Atom-ordering methods were evaluated using B3LYP. *Method 1* yielded an 80% success rate while *methods 0* and *2* were successful for 70% of the data set. *Method 0* (or the most successful alternative where *method 0* was not successful) was then applied for calculations with the other functionals. Because each method was suitable for different types of geometries, overall the three methods covered all of the pericyclic reactions tested (see Supporting Information for details).

For all successful executions, A.V.E.D.A. tabulates the molecular dipole moments ($\vec{\mu}$) and optimized local-minimum and transition-state electronic and free energies in CSV files (compiled in Table 1 for Reactions 1 and 2). The RMSD distortion from the zero-field geometry is also reported each OEF strength to quantify structural changes. Finally, A.V.E.D.A. plots the effective activation energy ($\Delta E^{\ddagger}$ or $\Delta G^{\ddagger}$, kcal/mol) as a function of OEF magnitude (a.u.) from the tabulated energies (Figure 3).

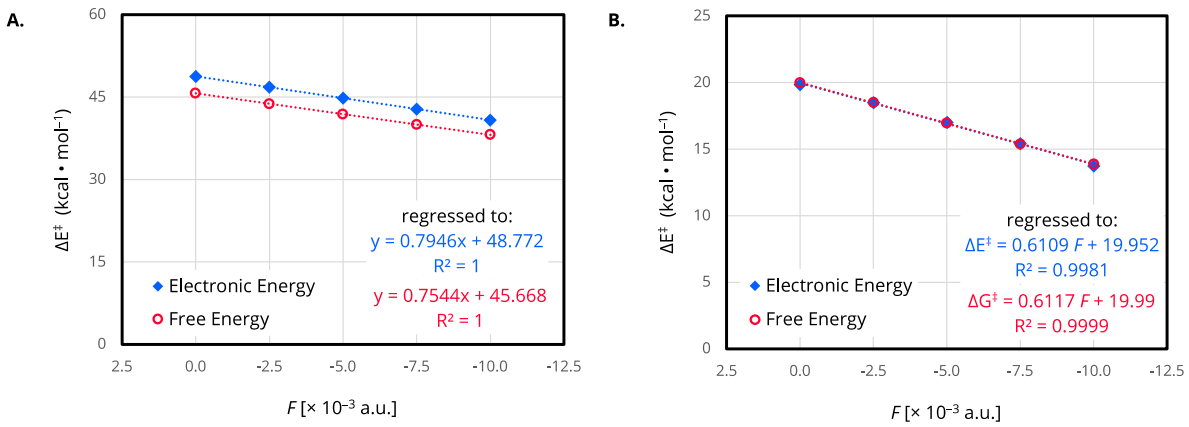

Figure 3. Plot of the effective activation energy ($\Delta E^{\ddagger}$ or $\Delta G^{\ddagger}$, kcal/mol) as a function of OEF magnitude for (A.) Reaction 1 and (B.) Reaction 2 computed at the B3LYP-D3/def2-TZVP level of theory (gas phase, 298 K). Both uncorrected electronic energies (blue diamonds) and corrected electronic and thermal free energies (red circles) are reported.

Table 1. Summary of A.V.E.D.A. output data for (A.) Reaction 1 and (B.) Reaction 2 computed at the B3LYP-D3/def2-TZVP level of theory (gas phase, 298 K).

A. Reaction 1					
Dipole Moments (μ) [debeye]					
μ_{Int} [x,y,z]	[0.2481, –1.8900, -0.0889]			$\|\|\mu_{Int}\|\|$	1.9083
μ_{TS} [x,y,z)	[0.3813, 1.2430, 0.6952]			$\|\|\mu_{TS}\|\|$	1.4744
μ_{rxn} [x,y,z]	[0.1332, 3.1330, 0.7841]			$\|\|\mu_{rxn}\|\|$	3.2324
Oriented Electric Field (F) [$\times 10^{-3}$ a.u.]					
	0	–2.5	–5.0	–7.5	–10.0
Electronic Energies (E)					
Int [a.u.]	–210.2570	–210.2553	–210.2541	–210.2532	–210.2527
TS [a.u.]	–210.1791	–210.1806	–210.1825	–210.1848	–210.1874
$\Delta E^{\ddagger}$ [kcal/mol]	48.88	46.89	44.90	42.91	40.93
$\Delta\Delta E^{\ddagger}$ [kcal/mol]	0	–1.99	–3.98	–5.97	–7.95
Free Energies (G)					
Int [a.u.]	–210.2011	–210.1996	–210.1985	–210.1978	–210.1974
TS [a.u.]	–210.1282	–210.1297	–210.1316	–210.1339	–210.1365
$\Delta G^{\ddagger}$ [kcal/mol]	45.75	43.85	41.95	40.07	38.22
$\Delta\Delta G^{\ddagger}$ [kcal/mol]	0.00	–1.91	–3.80	–5.68	–7.54
RMSD from Zero–Field [Å]					
Int	–	0.0023	0.0055	0.0092	0.0081
TS	–	0.0024	0.0049	0.0074	0.0098
B. Reaction 2					
Dipole Moments (μ) [debeye]					
μ_{Int} [x,y,z]	[–0.1313, –1.6860, 1.8263]			$\|\|\mu_{Int}\|\|$	2.4890
μ_{TS} [x,y,z)	[1.5291,–2.9343, 1.4541]			$\|\|\mu_{TS}\|\|$	3.6142
μ_{rxn} [x,y,z]	[1.6604,–1.2483,–0.3722]			$\|\|\mu_{rxn}\|\|$	2.1104
Oriented Electric Field (F) [$\times 10^{-3}$ a.u.]					
	0	–2.5	–5.0	–7.5	–10.0
Electronic Energies (E)					
Int [a.u.]	–669.5006	–669.5016	–669.5035	–669.5064	–669.5104
TS [a.u.]	–669.4689	–669.4721	–669.4764	–669.4819	–669.4885
$\Delta E^{\ddagger}$ [kcal/mol]	19.84	18.48	17.01	15.42	13.73
$\Delta\Delta E^{\ddagger}$ [kcal/mol]	0.00	–1.36	–2.83	–4.42	–6.10
Free Energies (G)					
Int [a.u.]	–669.3190	–669.3200	–669.3221	–669.3253	–669.3298
TS [a.u.]	–669.2872	–669.2906	–669.2951	–669.3008	–669.3077
$\Delta G^{\ddagger}$ [kcal/mol]	19.97	18.49	16.93	15.38	13.88
$\Delta\Delta G^{\ddagger}$ [kcal/mol]	0.00	–1.48	–3.04	–4.59	–6.09
RMSD from Zero–Field [Å]					
Int	–	0.0038	0.0074	0.0076	0.0190
TS	–	0.0195	0.0699	0.1121	0.1613

2.5 Validating the Reaction Axis Assumption

Following program workflow development and testing, the key assumption underlying this ersatz was validated by considering the electric field orientation with respect to $\hat{\mu}^{\ddagger}$ for reaction 1. The A.V.E.D.A. algorithm was adapted to apply an electric field along 20 vectors distributed over a unit sphere, each scaled to a magnitude of 5.0×10^{-3} a.u. The field-perturbed local-minimum and transition-state structures and energies were then computed. As expected, the lowest $\Delta E^{\ddagger}$ was realized along $-\hat{\mu}^{\ddagger}$, while fields that increased $\Delta E^{\ddagger}$ were found when the applied field included a $+\hat{\mu}^{\ddagger}$component; see Supporting Information for visualization. Note that the Gaussian positive field direction is opposite to physics convention; thus applying an electric field along $-\hat{\mu}^{\ddagger}$ represents alignment between the field and reaction axis of the given transformation and stabilization of the dipole moment.[13] These data thus validated the assumption, made in developing the program workflow, that the optimally oriented fields project along $\hat{\mu}^{\ddagger}$.

2.6 Relating OEF Effects to Dipoles and Geometries

A relationship between the predicted rate enhancement and the magnitude of $\Delta\vec{\mu}^{\ddagger}$ emerged from the pericyclic reaction data set. Across levels of theory, the change in activation energy OEF (vs the zero-field case) with application of an oriented electric field (10.0×10^{-3} a.u.) demonstrated a strong linear correlation with the reaction dipole magnitude (Figure 5), thus implying that reactions with larger $\left\|\vec{\mu}^{\ddagger}\right\|$ are more susceptible to acceleration by an OEF. The strongest correlation ($R^2 = 0.987$) was observed with the electronic energy difference ($\Delta\Delta E^{\ddagger}$, Figure 5A), with only a slightly weaker fit ($R^2 = 0.9764$) observed when considering the computed enthalpy difference ($\Delta\Delta H^{\ddagger}$, Figure 5B). However, significantly increased scatter ($R^2 = 0.946$), especially involving cases with large $\left\|\vec{\mu}^{\ddagger}\right\|$, was observed upon considering the computed free energy difference ($\Delta\Delta G^{\ddagger}$, Figure 5C). This result arises from the entropic impacts of field-induced

geometric changes, which may be non-intuitive to predict. This variable behavior thus highlights the utility of full DFT-level evaluation of a reaction of interest, rather than considering the reaction dipole difference alone.

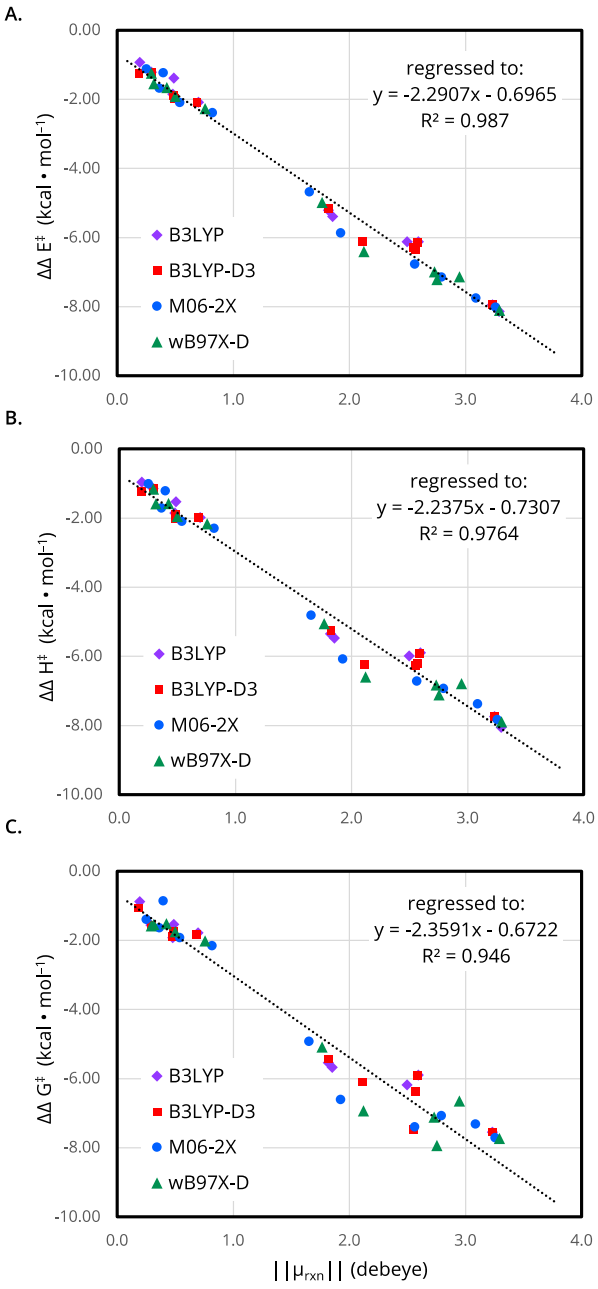

Figure 4. Correlation between net reaction dipole moment ($\vec{\mu}^{\ddagger}$or $\vec{\mu}_{rxn}$) and change in effective activation energy for the model reaction set described by the (A.) uncorrected electronic energy

difference ($\Delta\Delta E^{\ddagger}$), (B.) thermally-corrected enthalpy difference ($\Delta\Delta H^{\ddagger}$), and (C.) thermally-corrected free energy difference ($\Delta\Delta G^{\ddagger}$). Results computed in the gas phase at 298 K using B3LYP (purple diamonds), B3LYP-D3 (red squares), M06-2X (blue circles), and ωB97X-D (green triangles) with the def2-TZVP basis set.

To better understand the nature of the geometric changes arising from application of the electric field, molecular geometries were thus evaluated for Reaction 2 as a case study. Although geometric perturbations were observed in the presence of an applied field for both the local-minimum and transition-state structures, the effects in the transition state were substantially greater, reflected in slight lengthening of the breaking C–C bond (Figure 4A, Δr_{CC} = + 0.05 Å) and substantial lengthening of the forming C–O bond (Figure 4B, Δr_{CO} = + 0.274 Å) over the 0–10 × 10^{-3} a.u. range. Taken together, these geometric changes reflect a shift towards an earlier, less-associative transition state, as depicted by the trend toward the diagonal in the More O'Ferrall–Jenks plot (Figure 4C).[61] These findings further highlight that one of the strengths of a full DFT-optimization for evaluating electric field effects (as compared to the rapid, Taylor series expansion approximation[44]) is the wealth of resulting structural insight.

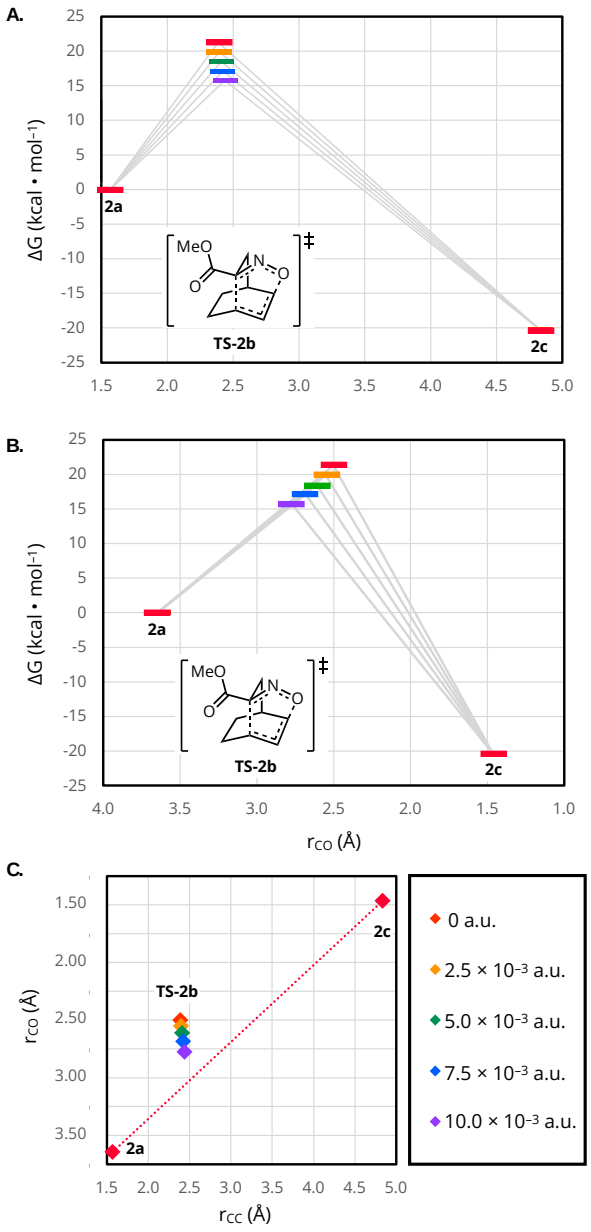

Figure 5. Field-induced geometric distortions in the transition-state structure for Reaction 2 represented as reaction coordinate diagrams reflecting changing (A.) C–C and (B.) C–O bond lengths as well as (C.) a More O'Ferrall–Jenks representation. Calculations performed at the B3LYP-D3/def2-TZVP level of theory (gas phase, 298 K). Zero-field (red) and applied fields of 2.5 (orange), 5.0 (green), 7.5 (blue), and 10.0 (purple) × 10^{-3} shown.

2.7 Scope of A.V.E.D.A.

Although A.V.E.D.A. was developed and tested on the pericyclic reaction training data set, its design facilitates broad applications. To demonstrate transferability, A.V.E.D.A. was implemented to study potential electric field effects on alternative (non-pericyclic) reaction classes including electrophilic addition and concerted metallation-deprotonation (CMD) mechanisms (see Supporting Information).[62] Computations have no constraint on system size, computer resource caps, or run time limits (barring those controlled by SLURM for the user's computing cluster). While optimization times depend on system size, the local A.V.E.D.A. calculations and processes remain virtually unchanged. Furthermore, multiple predefined atom ordering methods, variable level of theory, detailed documentation, and fully open-source software enable broad customization for computationally challenging instances. The simple initiation requirements and automated mathematical processing thus increase the accessibility of OEF studies to students and computational non-experts, thereby providing opportunities for increased contribution from the synthetic community.

3. CONCLUSIONS

The computational workflow described herein offers a simple tool for evaluation of chemical reactions in optimally oriented electric fields using density functional theory. A.V.E.D.A. is controlled by a one-time command, making the program highly accessible to computational non-experts. Results are discussed for a set of pericyclic reaction case studies, for which significant barrier reduction is predicted as a function of electric fields application along the $\vec{\mu}^{\ddagger}$ dipole difference vector. Structural changes due to the electric fields are considered, in addition to the relationship between dipole moment magnitude and absolute barrier reduction. These insights bolster the promise of OEF applications to modulate chemical reactivity and improve accessibility of computational tools to support this effort.

4. EXPERIMENTAL

Computational Methods. The complete workflow for all A.V.E.D.A. processes was developed in Python 3 and Bash script intended for use on a computing cluster running a Linux operating system and the SLURM scheduling protocol.[46] The Gaussian 16 module is loaded and executed for all density functional theory calculations throughout the workflow.[63] Structural analysis, visualization, and presentation was facilitated by Avogadro,[64, 65] UCSF Chimera,[66] and CYLview.[67] Optimizations were completed in the gas phase at 298 K using were evaluated using four different functionals (B3LYP, B3LYP-D3, M06-2X, and ωB97X-D) [54-56, 59, 60] and Weigend's triple-ζ basis set, def2-TZVP.[52, 53] However, users may request any Gaussian-standard functional at instantiation. All reported structures were confirmed with normal vibrational mode analyses yielding zero imaginary frequencies for local minima and a single imaginary frequency for transition states. Uncorrected electronic energies and corrected, thermal and electronic free energies are reported. The complete pericyclic data set geometries—optimized at all field strengths for each successful atom ordering method—may be found in the Supporting Information.

Implementation. Each instance of A.V.E.D.A. requires intermediate and transition state geometries in *.xyz* format, with corresponding atoms numbered consistently, to be in the same directory as the *start.sh* script and Program folder. When called, this script handles all setup and execution of the A.V.E.D.A. workflow and thus must be provided with job-specific user arguments. First, charge and multiplicity must be entered corresponding to the overall charge and electron configuration of the given transformation. The desired level of theory is indicated with a functional and basis set argument as well as the method for atom reordering (see Results and Discussion for details). Computing resources are allocated from SLURM by the desired number of processors and compute node. Finally, the user specifies to output electronic energies only

(keyword *nofreq*) or vibrationally corrected free energies (keyword *freq*, recommended). In the event that users bypass the frequency analysis to increase computational efficiency at the optimization stage, users are strongly encouraged to implement ex post facto frequency calculations and/or intrinsic reaction coordinate analyses. These are necessary to validate the stationary points identified and obtain physically meaningful corrected enthalpy and free-energy terms. Note, all input parameters must be satisfied or A.V.E.D.A. will return an error and stop instantiation. A.V.E.D.A. may be installed, edited, modified, and distributed, protected under the open source MIT License, from the Kennedy laboratory GitHub repository page.[68]

5. ASSOCIATED CONTENT

Supporting Information Available

The following files are available free of charge.

- Supplementary figures; output and energies for all model reaction; and extended discussion (PDF)
- Coordinates of computed structures (XYZ)

6. AUTHOR INFORMATION

Corresponding Author

C. Rose Kennedy — orcid.org/0000-0003-3681-819X; Email: c.r.kennedy@rochester.edu

Other Authors

Dalton Hanaway — orcid.org/0000-0003-2111-1773

Author Contributions

This manuscript was written with contributions from both authors.

Funding Sources

The authors thank the University of Rochester for financial support of this research. D.H. acknowledges the University of Rochester, Department of Chemistry, Dean Marvin Summer Research Fellowship.

Notes

The authors declare no competing financial interest.

7. ACKNOWLEDGEMENT

The authors thank Prof. Ignacio Franco (University of Rochester), Prof. Pengfei Huo (University of Rochester), Prof. Andrew White (University of Rochester), and Aliza Panjwani (University of Rochester) for helpful discussions. Computations were performed on the Center for Integrated Research Computing (CIRC) BlueHive cluster at the University of Rochester; the authors are grateful for the CIRC team for their guidance.

8. REFERENCES

1. Shaik, S.; de Visser, S. P.; Kumar, D. External Electric Field Will Control the Selectivity of Enzymatic-Like Bond Activations. *J. Am. Chem. Soc.* **2004**, *126*, 11746–11749. DOI: 10.1021/ja047432k
2. Shaik, S.; Ramanan, R.; Danovich, D.; Mandal, D. Structure and reactivity/selectivity control by oriented-external electric fields. *Chem. Soc. Rev.* **2018**, *47*, 5125–5145. DOI: 10.1039/C8CS00354H
3. Shaik, S.; Danovich, D.; Joy, J.; Wang, Z.; Stuyver, T. Electric-Field Mediated Chemistry: Uncovering and Exploiting the Potential of (Oriented) Electric Fields to Exert Chemical Catalysis and Reaction Control. *J. Am. Chem. Soc.* **2020**, *142*, 12551–12562. DOI: 10.1021/jacs.0c05128
4. Shaik, S.; Mandal, D.; Ramanan, R. Oriented electric fields as future smart reagents in chemistry. *Nat. Chem.* **2016**, *8*, 1091–1098. DOI: 10.1038/nchem.2651

5. Warshel, A. Electrostatic basis of structure-function correlation in proteins. *Acc. Chem. Res.* **1981**, *14*, 284–290. DOI: 10.1021/ar00069a004
6. Warshel, A.; Sharma, P. K.; Kato, M.; Xiang, Y.; Liu, H.; Olsson, M. H. M. Electrostatic Basis for Enzyme Catalysis. *Chem. Rev.* **2006**, *106*, 3210–3235. DOI: 10.1021/cr0503106
7. Kollman, P. A.; Kuhn, B.; Donini, O.; Perakyla, M.; Stanton, R.; Bakowies, D. Elucidating the Nature of Enzyme Catalysis Utilizing a New Twist on an Old Methodology: Quantum Mechanical−Free Energy Calculations on Chemical Reactions in Enzymes and in Aqueous Solution. *Acc. Chem. Res.* **2001**, *34*, 72-79. DOI: 10.1021/ar000032r
8. Martí, S.; Andrés, J.; Moliner, V.; Silla, E.; Tuñón, I.; Bertrán, J. Preorganization and Reorganization as Related Factors in Enzyme Catalysis: The Chorismate Mutase Case. *Chem. Eur. J.* **2003**, *9*, 984–991. DOI: 10.1002/chem.200390121
9. Szefczyk, B.; Mulholland, A. J.; Ranaghan, K. E.; Sokalski, W. A. Differential Transition-State Stabilization in Enzyme Catalysis: Quantum Chemical Analysis of Interactions in the Chorismate Mutase Reaction and Prediction of the Optimal Catalytic Field. *J. Am. Chem. Soc.* **2004**, *126*, 16148–16159. DOI: 10.1021/ja049376t
10. Martí, S.; Roca, M.; Andrés, J.; Moliner, V.; Silla, E.; Tuñón, I.; Bertrán, J. Theoretical insights in enzyme catalysis. *Chem. Soc. Rev.* **2004**, *33*, 98-107. DOI: 10.1039/B301875J
11. Hennefarth, M. R.; Alexandrova, A. N. Advances in optimizing enzyme electrostatic preorganization. *Curr. Opin. Struct. Biol.* **2022**, *72*, 1–8. DOI: 10.1016/j.sbi.2021.06.006
12. Suydam, I. T.; Snow, C. D.; Pande, V. S.; Boxer, S. G. Electric Fields at the Active Site of an Enzyme: Direct Comparison of Experiment with Theory. *Science* **2006**, *313*, 200–204. DOI: 10.1126/science.1127159
13. Fried, S. D.; Bagchi, S.; Boxer, S. G. Extreme electric fields power catalysis in the active site of ketosteroid isomerase. *Science* **2014**, *346*, 1510–1514. DOI: 10.1126/science.1259802
14. Fafarman, A. T.; Sigala, P. A.; Schwans, J. P.; Fenn, T. D.; Herschlag, D.; Boxer, S. G. Quantitative, directional measurement of electric field heterogeneity in the active site of ketosteroid isomerase. *Proc. Natl. Acad. Sci. U.S.A.* **2012**, *109*, E299–E308. DOI: 10.1073/pnas.1111566109
15. Wu, Y.; Boxer, S. G. A Critical Test of the Electrostatic Contribution to Catalysis with Noncanonical Amino Acids in Ketosteroid Isomerase. *J. Am. Chem. Soc.* **2016**, *138*, 11890-11895. DOI: 10.1021/jacs.6b06843
16. Wu, Y.; Fried, S. D.; Boxer, S. G. A Preorganized Electric Field Leads to Minimal Geometrical Reorientation in the Catalytic Reaction of Ketosteroid Isomerase. *J. Am. Chem. Soc.* **2020**, *142*, 9993–9998. DOI: 10.1021/jacs.0c00383
17. Delley, M. F.; Nichols, E. M.; Mayer, J. M. Interfacial Acid–Base Equilibria and Electric Fields Concurrently Probed by In Situ Surface-Enhanced Infrared Spectroscopy. *J. Am. Chem. Soc.* **2021**, *143*, 10778–10792. DOI: 10.1021/jacs.1c05419
18. Sarkar, S.; Maitra, A.; Banerjee, S.; Thoi, V. S.; Dawlaty, J. M. Electric Fields at Metal–Surfactant Interfaces: A Combined Vibrational Spectroscopy and Capacitance Study. *J. Phys. Chem. B.* **2020**, *124*, 1311–1321. DOI: 10.1021/acs.jpcb.0c00560
19. Wesley, T. S.; Román-Leshkov, Y.; Surendranath, Y. Spontaneous Electric Fields Play a Key Role in Thermochemical Catalysis at Metal−Liquid Interfaces. *ACS Cent. Sci.* **2021**, *7*, 1045–1055. DOI: 10.1021/acscentsci.1c00293

20. Meir, R.; Chen, H.; Lai, W.; Shaik, S. Oriented Electric Fields Accelerate Diels–Alder Reactions and Control the endo/exo Selectivity. *ChemPhysChem* **2010**, *11*, 301-310. DOI: 10.1002/cphc.200900848
21. Bhattacharyya, K.; Karmakar, S.; Datta, A. External electric field control: driving the reactivity of metal-free azide–alkyne click reactions. *Phys. Chem. Chem. Phys.* **2017**, *19*, 22482-22486. DOI: 10.1039/C7CP04202G
22. Wang, Z.; Danovich, D.; Ramanan, R.; Shaik, S. Oriented-External Electric Fields Create Absolute Enantioselectivity in Diels–Alder Reactions: Importance of the Molecular Dipole Moment. *J. Am. Chem. Soc.* **2018**, *140*, 13350–13359. DOI: 10.1021/jacs.8b08233
23. Mandal, S.; Datta, A. Metal-free Kinugasa reaction catalyzed by external electric field. *J. Phys. Org. Chem.* **2022**, *35*, e4327. DOI: 10.1002/poc.4327
24. Aragonès, A. C.; Haworth, N. L.; Darwish, N.; Ciampi, S.; Bloomfield, N. J.; Wallace, G. G.; Diez-Perez, I.; Coote, M. L. Electrostatic catalysis of a Diels–Alder reaction. *Nature* **2016**, *531*, 88–91. DOI: 10.1038/nature16989
25. Huang, X.; Tang, C.; Li, J.; Chen, L.-C.; Zheng, J.; Zhang, P.; Le, J.; Li, R.; Li, X.; Liu, J.; Yang, Y.; Shi, J.; Chen, Z.; Bai, M.; Zhang, H.-L.; Xia, H.; Cheng, J.; Tian, Z.-Q.; Hong, W. Electric field–induced selective catalysis of single-molecule reaction. *Sci. Adv.* **2019**, *5*, eaaw3072. DOI: 10.1126/sciadv.aaw3072
26. Orchanian, N. M.; Guizzo, S.; Steigerwald, M. L.; Nuckolls, C.; Venkataraman, L. Electric-field-induced coupling of aryl iodides with a nickel(0) complex. *Chem. Commun.* **2022**. DOI: 10.1039/D2CC03671A
27. Zang, Y.; Zou, Q.; Fu, T.; Ng, F.; Fowler, B.; Yang, J.; Li, H.; Steigerwald, M. L.; Nuckolls, C.; Venkataraman, L. Directing isomerization reactions of cumulenes with electric fields. *Nat. Commun.* **2019**, *10*, 4482. DOI: 10.1038/s41467-019-12487-w
28. Alemani, M.; Peters, M. V.; Hecht, S.; Rieder, K.-H.; Moresco, F.; Grill, L. Electric Field-Induced Isomerization of Azobenzene by STM. *J. Am. Chem. Soc.* **2006**, *128*, 14446–14447. DOI: 10.1021/ja065449s
29. Che, F.; Gray, J. T.; Ha, S.; Kruse, N.; Scott, S. L.; McEwen, J.-S. Elucidating the Roles of Electric Fields in Catalysis: A Perspective. *ACS Catal.* **2018**, *8*, 5153–5174. DOI: 10.1021/acscatal.7b02899
30. Clarys, T.; Stuyver, T.; De Proft, F.; Geerlings, P. Extending conceptual DFT to include additional variables: oriented external electric field. *Phys. Chem. Chem. Phys.* **2021**, *23*, 990–1005. DOI: 10.1039/D0CP05277A
31. Gorin, C. F.; Beh, E. S.; Kanan, M. W. An Electric Field–Induced Change in the Selectivity of a Metal Oxide–Catalyzed Epoxide Rearrangement. *J. Am. Chem. Soc.* **2012**, *134*, 186–189. DOI: 10.1021/ja210365j
32. Gorin, C. F.; Beh, E. S.; Bui, Q. M.; Dick, G. R.; Kanan, M. W. Interfacial Electric Field Effects on a Carbene Reaction Catalyzed by Rh Porphyrins. *J. Am. Chem. Soc.* **2013**, *135*, 11257-11265. DOI: 10.1021/ja404394z
33. Ciampi, S.; Darwish, N.; Aitken, H. M.; Díez-Pérez, I.; Coote, M. L. Harnessing electrostatic catalysis in single molecule, electrochemical and chemical systems: a rapidly growing experimental tool box. *Chem. Soc. Rev.* **2018**, *47*, 5146-5164. DOI: 10.1039/C8CS00352A
34. Léonard, N. G.; Dhaoui, R.; Chantarojsiri, T.; Yang, J. Y. Electric Fields in Catalysis: From Enzymes to Molecular Catalysts. *ACS Catal.* **2021**, *11*, 10923–10932. DOI: 10.1021/acscatal.1c02084

35. Weberg, A. B.; Murphy, R. P.; Tomson, N. C. Oriented internal electrostatic fields: an emerging design element in coordination chemistry and catalysis. *Chem. Sci.* **2022**, *13*, 5432–5446. DOI: 10.1039/D2SC01715F
36. Reath, A. H.; Ziller, J. W.; Tsay, C.; Ryan, A. J.; Yang, J. Y. Redox Potential and Electronic Structure Effects of Proximal Nonredox Active Cations in Cobalt Schiff Base Complexes. *Inorg. Chem.* **2017**, *56*, 3713–3718. DOI: 10.1021/acs.inorgchem.6b03098
37. Chantarojsiri, T.; Reath, A. H.; Yang, J. Y. Cationic Charges Leading to an Inverse Free-Energy Relationship for N−N Bond Formation by MnVI Nitrides. *Angew. Chem. Int. Ed.* **2018**, *57*, 14037-14042. DOI: 10.1002/anie.201805832
38. Chantarojsiri, T.; Ziller, J. W.; Yang, J. Y. Incorporation of redox-inactive cations promotes iron catalyzed aerobic C–H oxidation at mild potentials. *Chem. Sci.* **2018**, *9*, 2567–2574. DOI: 10.1039/C7SC04486K
39. Kang, K.; Fuller, J.; Reath, A. H.; Ziller, J. W.; Alexandrova, A. N.; Yang, J. Y. Installation of internal electric fields by non-redox active cations in transition metal complexes. *Chem. Sci.* **2019**, *10*, 10135-10142. DOI: 10.1039/C9SC02870F
40. Idris, N. S.; Barlow, J. M.; Chabolla, S. A.; Ziller, J. W.; Yang, J. Y. Synthesis and redox properties of heterobimetallic Re(bpyCrown-M)(CO)3Cl complexes, where M = Na+, K+, Ca2+, and Ba2+. *Polyhedron* **2021**, *208*, 115385. DOI: 10.1016/j.poly.2021.115385
41. Barlow, J. M.; Ziller, J. W.; Yang, J. Y. Inhibiting the Hydrogen Evolution Reaction (HER) with Proximal Cations: A Strategy for Promoting Selective Electrocatalytic Reduction. *ACS Catal.* **2021**, *11*, 8155–8164. DOI: 10.1021/acscatal.1c01527
42. Léonard, N. G.; Chantarojsiri, T.; Ziller, J. W.; Yang, J. Y. Cationic Effects on the Net Hydrogen Atom Bond Dissociation Free Energy of High-Valent Manganese Imido Complexes. *J. Am. Chem. Soc.* **2022**, *144*, 1503–1508. DOI: 10.1021/jacs.1c09583
43. Weberg, A. B.; McCollom, S. P.; Thierer, L. M.; Gau, M. R.; Carroll, P. J.; Tomson, N. C. Using internal electrostatic fields to manipulate the valence manifolds of copper complexes. *Chem. Sci.* **2021**, *12*, 4395-4404. DOI: 10.1039/D0SC06364A
44. Besalú-Sala, P.; Solà, M.; Luis, J. M.; Torrent-Sucarrat, M. Fast and Simple Evaluation of the Catalysis and Selectivity Induced by External Electric Fields. *ACS Catal.* **2021**, *11*, 14467–14479. DOI: 10.1021/acscatal.1c04247
45. Fleming, I. *Pericyclic Reactions*. Oxford University Press: 2015.
46. Note that the SLURM workload manager is the standard scheduling tool for computing clusters: Yoo, A. B.; Jette, M. A.; Grondona, M. In *SLURM: Simple Linux Utility for Resource Management*, Job Scheduling Strategies for Parallel Processing, Berlin, Heidelberg, Feitelson, D.; Rudolph, L.; Schwiegelshohn, U., Eds. Springer Berlin, Heidelberg, 2003; pp 44–60.
47. Andrés, J. L.; Lledós, A.; Duran, M.; Bertrán, J. Electric fields acting as catalysts in chemical reactions. An ab initio study of the walden inversion reaction. *Chem. Phys. Lett.* **1988**, *153*, 82–86. DOI: 10.1016/0009-2614(88)80136-2
48. Stuyver, T.; Danovich, D.; De Proft, F.; Shaik, S. Electrophilic Aromatic Substitution Reactions: Mechanistic Landscape, Electrostatic and Electric-Field Control of Reaction Rates, and Mechanistic Crossovers. *J. Am. Chem. Soc.* **2019**, *141*, 9719–9730. DOI: 10.1021/jacs.9b04982
49. Joy, J.; Stuyver, T.; Shaik, S. Oriented External Electric Fields and Ionic Additives Elicit Catalysis and Mechanistic Crossover in Oxidative Addition Reactions. *J. Am. Chem. Soc.* **2020**, *142*, 3836–3850. DOI: 10.1021/jacs.9b11507

50. Researchers in the United States who do not have access to Gaussian at their home institution may obtain access to computing resources through the National Science Foundation ACCESS program: *Advanced Cyberinfrastructure Coordination Ecosystem: Services & Support (ACCESS) program*. https://access-ci.org/ (accessed 2022-11-19).
51. *The PyMOL Molecular Graphics System,* Version 2.0 Schrödinger, LLC. https://pymol.org/2/ (accessed 2022-11-19).
52. Weigend, F. Accurate Coulomb-fitting basis sets for H to Rn. *Phys. Chem. Chem. Phys.* **2006**, *8*, 1057–1065. DOI: 10.1039/B515623H
53. Weigend, F.; Ahlrichs, R. Balanced basis sets of split valence, triple zeta valence and quadruple zeta valence quality for H to Rn: Design and assessment of accuracy. *Phys. Chem. Chem. Phys.* **2005**, *7*, 3297–3305. DOI: 10.1039/B508541A
54. Becke, A. D. Density-functional thermochemistry. III. The role of exact exchange. *J. Chem. Phys.* **1993**, *98*, 5648-5652. DOI: 10.1063/1.464913
55. Grimme, S.; Antony, J.; Ehrlich, S.; Krieg, H. A consistent and accurate ab initio parametrization of density functional dispersion correction (DFT-D) for the 94 elements H-Pu. *J. Chem. Phys.* **2010**, *132*, 154104. DOI: 10.1063/1.3382344
56. Zhao, Y.; Truhlar, D. G. The M06 suite of density functionals for main group thermochemistry, thermochemical kinetics, noncovalent interactions, excited states, and transition elements: two new functionals and systematic testing of four M06-class functionals and 12 other functionals. *Theor. Chem. Account* **2008**, *120*, 215–241. DOI: 10.1007/s00214-007-0310-x
57. Ess, D. H.; Houk, K. N. Activation Energies of Pericyclic Reactions: Performance of DFT, MP2, and CBS-QB3 Methods for the Prediction of Activation Barriers and Reaction Energetics of 1,3-Dipolar Cycloadditions, and Revised Activation Enthalpies for a Standard Set of Hydrocarbon Pericyclic Reactions. *J. Phys. Chem. A* **2005**, *109*, 9542–9553. DOI: 10.1021/jp052504v
58. Vermeeren, P.; Dalla Tiezza, M.; Wolf, M. E.; Lahm, M. E.; Allen, W. D.; Schaefer, H. F.; Hamlin, T. A.; Bickelhaupt, F. M. Pericyclic reaction benchmarks: hierarchical computations targeting CCSDT(Q)/CBS and analysis of DFT performance. *Phys. Chem. Chem. Phys.* **2022**, *24*, 18028–18042. DOI: 10.1039/D2CP02234F
59. Chai, J.-D.; Head-Gordon, M. Long-range corrected hybrid density functionals with damped atom–atom dispersion corrections. *Phys. Chem. Chem. Phys.* **2008**, *10*, 6615–6620. DOI: 10.1039/B810189B
60. Grimme, S. Semiempirical GGA-type density functional constructed with a long-range dispersion correction. *J. Comput. Chem.* **2006**, *27*, 1787–1799. DOI: 10.1002/jcc.20495
61. Anslyn, E. V.; Dougherty, D. A. *Modern Physical Organic Chemistry*. University Science Books: 2006; p. 410.
62. Wang, L.; Carrow, B. P. Oligothiophene Synthesis by a General C–H Activation Mechanism: Electrophilic Concerted Metalation–Deprotonation (eCMD). *ACS Catal.* **2019**, *9*, 6821–6836. DOI: 10.1021/acscatal.9b01195
63. Frisch, M. J.; Trucks, G. W.; Schlegel, H. B.; Scuseria, G. E.; Robb, M. A.; Cheeseman, J. R.; Scalmani, G.; Barone, V.; Petersson, G. A.; Nakatsuji, H.; Li, X.; Caricato, M.; Marenich, A. V.; Bloino, J.; Janesko, B. G.; Gomperts, R.; Mennucci, B.; Hratchian, H. P.; Ortiz, J. V.; Izmaylov, A. F.; Sonnenberg, J. L.; Williams-Young, D.; Ding, F.; Lipparini, F.; Egidi, F.; Goings, J.; Peng, B.; Petrone, A.; Henderson, T.; Ranasinghe, D.; Zakrzewski, V. G.; Gao, J.; Rega, N.; Zheng, G.; Liang, W.; Hada, M.; Ehara, M.; Toyota, K.; Fukuda,

R.; Hasegawa, J.; Ishida, M.; Nakajima, T.; Honda, Y.; Kitao, O.; Nakai, H.; Vreven, T.; Throssell, K.; Montgomery, J., J. A. ; Peralta, J. E.; Ogliaro, F.; Bearpark, M. J.; Heyd, J. J.; Brothers, E. N.; Kudin, K. N.; Staroverov, V. N.; Keith, T. A.; Kobayashi, R.; Normand, J.; Raghavachari, K.; Rendell, A. P.; Burant, J. C.; Iyengar, S. S.; Tomasi, J.; Cossi, M.; Millam, J. M.; Klene, M.; Adamo, C.; Cammi, R.; Ochterski, J. W.; Martin, R. L.; Morokuma, K.; Farkas, O.; Foresman, J. B.; Fox, D. J. *Gaussian 16, Revision A.03*, Gaussian, Inc.: Wallingford, CT, 2016.

64. *Avogadro: an open-source molecular builder and visualization tool.*, 1.2.0. https://avogadro.cc/ (accessed 2022-11-19)

65. Hanwell, M. D.; Curtis, D. E.; Lonie, D. C.; Vandermeersch, T.; Zurek, E.; Hutchison, G. R. Avogadro: an advanced semantic chemical editor, visualization, and analysis platform. *J. Cheminform.* **2012**, *4*, 17. DOI: 10.1186/1758-2946-4-17

66. Pettersen, E. F.; Goddard, T. D.; Huang, C. C.; Couch, G. S.; Greenblatt, D. M.; Meng, E. C.; Ferrin, T. E. UCSF Chimera—A visualization system for exploratory research and analysis. *J. Comput. Chem.* **2004**, *25*, 1605–1612. DOI: 10.1002/jcc.20084

67. Legault, C. Y. *CYLview 2.0*, Université de Sherbrooke: 2020. https://www.cylview.org (accessed 2022-11-19)

68. Hanaway, D. H.; Kennedy, C. R. *A.V.E.D.A.*, GitHub: 2022. https://github.com/kennedy-lab-ur/A.V.E.D.A. (accessed 2022-11-19)

TOC GRAPHIC